RSC Advances

ROYAL SOCIETY OF CHEMISTRY

www.rsc.org/advances

Cite this: DOI: 10.1039/c0xx00000x

www.rsc.org/xxxxxx

Full Paper

A uniformly porous 2D CN (1:1) network predicted by the first-principles calculations

Zhengzheng Chen[a], Pengfei Li*[,a], Chao Wu*[,a]

Received (in XXX, XXX) XthXXXXXXXXX 20XX, Accepted Xth XXXXXXXXX 20XX

DOI: 10.1039/b000000x

A novel 2D structure composed only of carbon and nitrogen elements at the molar ratio of 1:1 is predicted by the first-principles calculations. The basic structural units are 1,3,5-triazine molecules which trimerize and polymerize into a 2D network of semiconductor nature. Six triazine units comprise a hollow hexagon with a van der Waals hole diameter of about 2.4 Å, which is suitable for H_2 separation from larger molecules. Metal atoms of various sizes can strongly bind over the polynitrogen pore, which suggests that the 2D network is an ideal support for single-atom catalysis.

Introduction

Experimental production of few- and single-layer graphene (Figure 1a) has opened a new era of two dimensional (2D) materials.[1] *P*- or *n*-type doping of graphene with elements like boron or nitrogen can substantially vary its electronic structure, which greatly broadens its application potential in electronic devices.[2-6] For nitrogen doping, if the graphene's honeycomb lattice scaffold is preserved, stable structure with the highest nitrogen content is theoretically predicted to be C_3N (Figure 1b).[4] Therefore, carbon nitride (CN_x) materials with higher nitrogen concentration have to abandon the benzene-sized honeycomb lattice by taking other arrangements of nitrogen heterocyclic rings.[7-11] For example, the widely studied graphitic C_3N_4 prefers sp^2-bonded structure composed of heptazine motifs(Figure 1c).[11, 12] Pores in the layer accommodate the lone-pairs of the edge nitrogen atoms, whose mutual repulsions lead to corrugation of layers.[9, 11] Amazingly, these nitrogen-rich carbon materials not only have superior mechanical properties, e.g. hardness comparable to diamond,[7-9, 13, 14] but also exhibit unusually high catalytic performance, such as in oxygen evolution electrocatalysis.[15] More interestingly, analogous to graphitic C_3N_4, a series of porous sp^2-bonded structures with higher carbon (and with hydrogen) contents than C_3N have been synthesized by self-assembling triazine derivatives into covalent frameworks (Figure 1d),[12, 16-20] which have demonstrated good applications in CO_2 capture[21] and conversion[18], H_2 gas storage,[22] NH_3 sensing[23] and supporting transition metal catalysts.[24] However, a pure CN 2D material with a higher nitrogen content than C_3N, formally formed by trimerization of s-triazine molecules, is missing from reports neither of experimental nor theoretical nature.

In this work, we propose a *planar* CN (1:1 ratio) hexagonal network with each honeycomb consisting of six 1,3,5-tri-substituted s-triazines (Figure 2a). By using the first-principles simulations, we show that (1) the single-layer structure is a stable semiconductor, (2) its regular honeycomb pore size is suitable for H_2 gas separation from larger molecules like CH_4 or CO_2, and (3) using the inner circle nitrogen atoms, its pores are strong binding sites for a large variety of metal atoms. This CN network is expected to have great potentials in many areas including separation, catalysis, electronics, mechanics, etc.

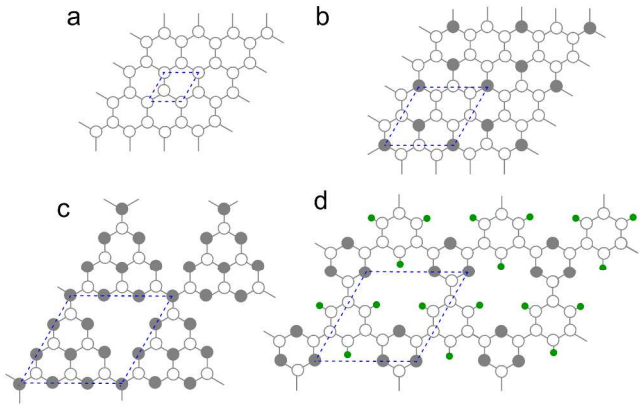

Figure 1.Representative single-layer carbon-(nitrogen-)based 2D materials. (a) Graphene. (b) The most stable configurationof C_3N.[4] (c) The most stable configuration of C_3N_4.[11, 25] (d) recently synthesized 1,3,5-tricyanobenzene-based covalent framework (CTF-0[18]). White dot is carbon, dark dot is nitrogen, and green dot is hydrogen. Dashed lines enclose the unit cells of the networks.

Methods

All calculations were performed with the VASP suite of programs.[26, 27] General gradient approximation (GGA) Perdew-Wang-91 (PW91) functional[28, 29] was employed in combination with the projected augmented wave method-based potentials[30, 31], which was used in most calculations. Heyd-Scuseria-Ernzerhof (HSE) exchange-correlation functional[32] was used for more accurate band structure calculations. In order to investigate the non-bonding interactions, both PW91 and the Perdew, Burke, and

Erzenhoff (PBE)[33] density functionals corrected with Grimme's long-range dispersion (density functional theory DFT-D2)[34] were employed to simulate the gas penetration process. Energy cut off was set to 450 eV. Single-layer 1 × 1 and √3 × √3 supercells (Figure 2) were calculated with spin polarization and lattice constants of 7.119 Å and 12.330 Å, respectively. The larger supercell (the dashed green parallelogram in Figure 2) was designed for checking the lateral interactions between neighbouring adsorbates.[35] A vacuum layer of 12 Å was inserted to ensure the calculations for the single layer were not disturbed by vertical image interactions. Monkhorst–Pack k-point mesh was chosen as 3 × 3 × 1. Gaussian smearing width was set to 0.1 eV. Structural optimization convergence was 0.01 eV/Å and the electronic structure convergence was 10^{-5} eV. The lattice constants of the metals were set to experimental values.[36] The minimum energy paths for gas diffusion through the pore were calculated by using the Climbing Image Nudged Elastic Band method with no fewer than 10 replicas.[37]

Results and discussion

A. Geometry and electronic structure

The CN network is completely planar even if the starting configuration was intentionally buckled, which is quite different from C_3N_4 structures,[11] where the nitrogen lone pair repulsions were attributed as the primary reason for the layer's corrugation. For the CN network, the phonon calculation at Γ point does show the planar structure is free of imaginary frequency. The insignificant effects of the lone pair repulsions in the CN layer to the geometry can be attributed to the longer distance of the neighbouring N-N lone pairs in the CN case (2.73 Å) compared to that in C_3N_4 structures (2.39 Å). The hexagonal hole surrounded by six trisubstituted s-triazine units has a diameter of 5.47 Å, the distance from one nitrogen atom to the opposite nitrogen atom across the hole (d_{N-N}), where all the lone pairs are nicely accommodated. The hole's van der Waals diameter is about 2.37 Å (d_{N-N} minus two nitrogen atoms' van der Waals radii).

The band structure suggests that the CN layer is a wide band gap semiconductor with a direct gap of 3.19 (HSE value; PW91 result: 1.69) eV at K point, while at Γ point, the gap is the biggest of 4.01 (PW91: 2.33) eV. The energy gap is smaller than other triazine-based networks.[38] Bands within 2 eV below the Fermi energy present flat character, suggesting that there are localized wavefunctions in CN network, which can be described more clearly by the projected density of states (PDOS). PDOS shows sharp double peaks right below the Fermi energy, indicating that these flat shallow bands are formed from the nitrogen lone pairs. Furthermore, lone pairs lie in *in-plane* orbitals (*σ* direction), suggesting the *σ*-donor nature of the pore. Nitrogen atoms take the sp^2 configuration and their lone pairs form the highest occupied band, which is further exhibited in the up-going band structure from Γ point to K point near the Fermi level. The filling of all the *in-plane* bonding orbitals implies the high stability of the structure.[39, 40] The p_z-*π* anitibonding delocalized orbitals form the lowest conduction band above the Fermi level, indicating the *π*-acceptor nature of the network.

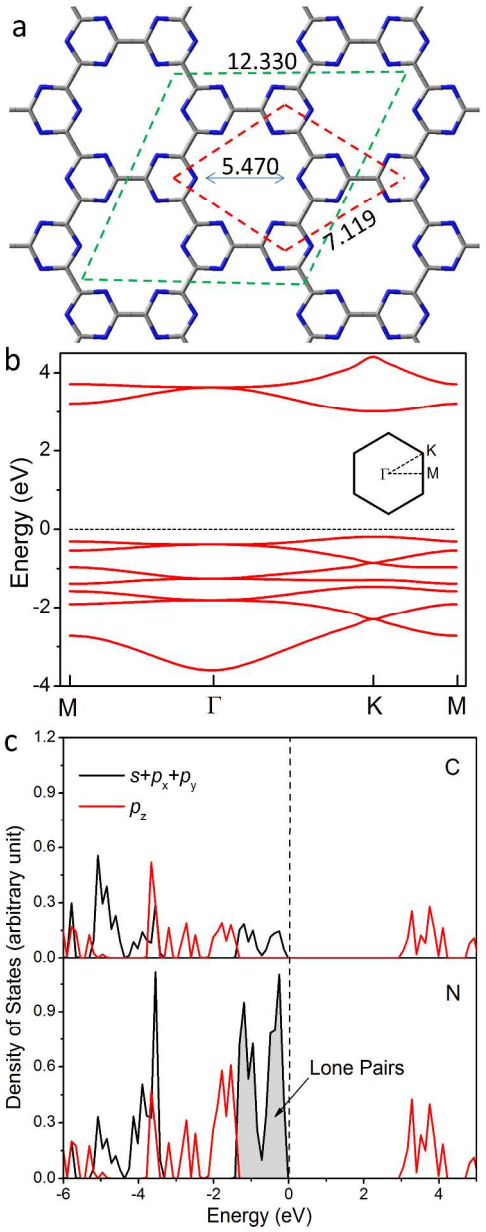

Figure 2.The 2D CN network (HSE results). (a)Top view of the optimized 2D CN network. √3 × √3 (green dashed parallelograms) and 1 × 1 (red dashed parallelograms) supercell models are used for calculations. (b) Band structure of the CN network. (c) Projected density of states of the CN network. The shaded area indicates the PDOS belonging to nitrogen lone pairs.

B. Gas separation

The uniformly distributed hexagonal-shaped pores and the small pore size of about 2.4 Å imply that the layered structure may be a good candidate for separating small hydrogen molecules from other larger molecules.[41] We calculated the diffusion barriers of a few key gases (H_2, CH_4, and CO_2) that are relevant to important industrial processes like syngas generation and natural gas purification.

The non-covalent interactions between the CN layer and the gas molecules may be important in obtaining a correct picture of energetics for the diffusion process. DFT corrected with

empirical dispersion term (DFT-D) is known to provide quantitatively more accurate description of the weak intermolecular interactions.[42, 43] To check the dispersion correction effect quantitatively, we employed four density functionals: PW91, PBE, PW91-D, and PBE-D to calculate the H_2 and CH_4 penetration barrier (Table 1). The barrier difference brought by the added dispersion term is quite small: For H_2, $\Delta E_{barrier}$ (GGA vs. GGA-D) is only 0.01 eV. For CH_4, $\Delta E_{barrier}$ increases to 0.06-0.07 eV. Similarly, Jiang and coworkers' reported less than 0.1 eV difference along the entire potential energy curves of H_2 passing through porous graphene sheets with different pore sizes when comparing PBE and the Rutgers-Chalmers van der Waals density functional (vdW-DF).[41] The limited effect of the dispersion correction may be explained by the interaction distances that we are interested in. For longer distance interactions, such like π-π stacking[42, 43] (> 3.3 Å, e.g. graphite interlayer distances), corrections with non-bonding interactions are essential. However, for shorter distances such as the diffusion barriers (< 3 Å) this kind of correction seems less crucial.

Table 1. Gas diffusion barriers (eV) through the CN layer.

Gas	PW91	PW91-D	PBE	PBE-D
H_2	0.31	0.32	0.36	0.35
CH_4	1.72	1.79	1.79	1.85

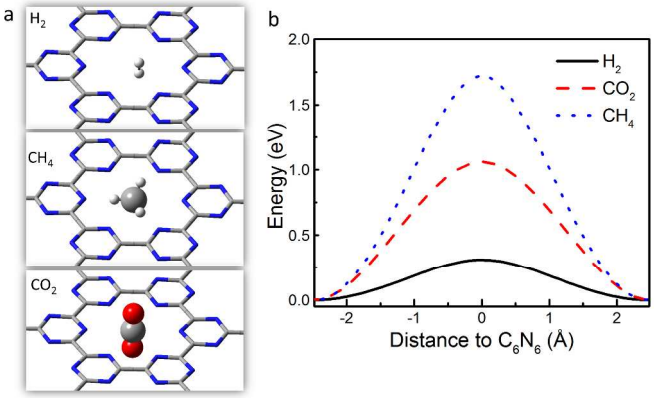

Figure 3.Transition pathways of gases (H_2, CH_4, and CO_2) through the CN layer (PW91 results). (a) Perspective view of transition states. For clarity, only one hexagonal pore is shown to illustrate the penetration geometry. (b) Minimum energy pathways. The lines only serve as a guide.

Table 1 also shows that different GGA functionals present consistent results. For H_2 and CH_4, the difference of penetration barrier between PW91 and PBE is 0.05 eV and 0.07 eV, respectively. Here, we mainly focus on the relative penetration capabilities, *i.e.*, selectivity, among the gas molecules, thus only PW91 was used for calculating the complete transition pathways for the three gases (Figure 3). The diffusion barriers for the three gases (H_2, CH_4, and CO_2) are 0.31, 1.72, and 1.05 eV, respectively. Notably, CO_2 has to adopt a vertical configuration when passing through the pore. Particularly, the nitrogen-rich pore expels the CH_4 molecule to such an extent that the network is virtually impenetrable for CH_4 under normal conditions. The barriers for H_2 and CH_4 penetration are comparable to the case of all-hydrogen passivated porous graphene when two neighbouring benzene units are removed (0.15 and 1.45 eV, vdW-DF values, van der Waals pore diameter 2.5 Å),[41] but are significantly larger than that of graphdiyne (0.10 and 0.72 eV, PBE-D values, van der Waals pore diameter is 3.8 Å).[44]Assuming the Arrhenius type kinetics, at 300 K, the H_2:CH_4:CO_2 diffusion rate ratio is estimated to be 10^{23}:1:10^{12}, which shows good selectivity of hydrogen over the other two gases. Additionally, the selectivity between CH_4 and CO_2 is also pretty high 1:10^{12}, comparable to some well-designed nanotube system.[45] The estimated frequency at room temperature for H_2 passing through is 10^8 per second if the rate constant prefactor is taken to be 10^{13} s^{-1}, suggesting a highly efficient hydrogen separation capability.

C. Binding to metals

Carbon-based 2D materials are promising in many application aspects. However, their potential in catalysis is usually limited by the unreactive nature of carbon itself, which is essential to the stability of the scaffold. Surprisingly, doping carbon-based nano materials with catalytically active species like nitrogen can sometimes bring extraordinary catalytic performance comparable to Pt (e.g. in oxygen reduction reaction).[46-48] In the CN network, there is naturally a circle of nitrogen atoms surrounding the hole, thus both catalytic centres and reaction space are readily available. Moreover, due to the *σ*-donating nature of the nitrogen lone pairs and the *π*-accepting nature of the network which facilitate both *σ*-bonding and *π*-backbonding, the pores are born to be ideal binding sites for many metal atoms.

Table 2. Binding energy of metal atoms with the CN layer.[a]

Metal	Atomic radius (Å)[b]	binding energy (eV)[c]	shortest $d_{N\text{-}metal}$(Å)	magnetic moments (μ_B)
Li	1.45	-2.9	2.21	0.0
K	2.20	-3.2	2.73	0.0
Rb	2.35	-3.0	2.90	0.0
Cs	2.60	-3.0	3.04	0.0
Ba	2.15	-5.3	2.75	0.0
Sc	1.60	-3.3	2.20	0.0
Zr	1.55	-2.2	2.29	1.2
Fe	1.40	0.7	1.99	3.7
Ru	1.30	2.6	2.30	3.6
Ir	1.35	1.7	2.72	0.0
Ni	1.35	0.5	1.93	1.5
Pd	1.40	1.2	2.72	0.9
Pt	1.35	1.2	2.72	1.2
Cu	1.35	0.4	2.02	0.0
Au	1.35	1.1	2.45	0.1

a. At the pore position, with 100% pore filled.[35]

b. Values taken from reference [49].

c. $E_{binding} = E_{metal\text{-}CN} - E_{CN} - E_{metal\ bulk}$ (PW91 results).

We tested a series of neutral metal atoms by calculating their interactions with the CN layer and the results are summarized in Table 2. In principle, there are two possible binding positions: over a s-triazine unit or over a pore (Figure 4a and 4b). The binding at the latter is calculated to be much stronger even for

small atoms. For example, binding energy differences for Li and K ($dE_{binding} = E_{binding@pore} - E_{binding@triazine}$) are -3.09 and -2.78 eV, respectively. For other metal atoms, only the binding over the pore was calculated. Li atom is small and binds more closely to one side of the pore (Figure 4b). K and similar sized atoms sit in the center of the pore (Figure 4c and 4d). When the atom's size is too big to be situated in the pore plane, it buckles out. For example, for Cs, the buckling is over 1Å (Figure 4f). Overall, the optimized geometries (Table 2, bond length column) show that the pore of the CN layer is a decent adsorption sites for all metals considered in the present work.

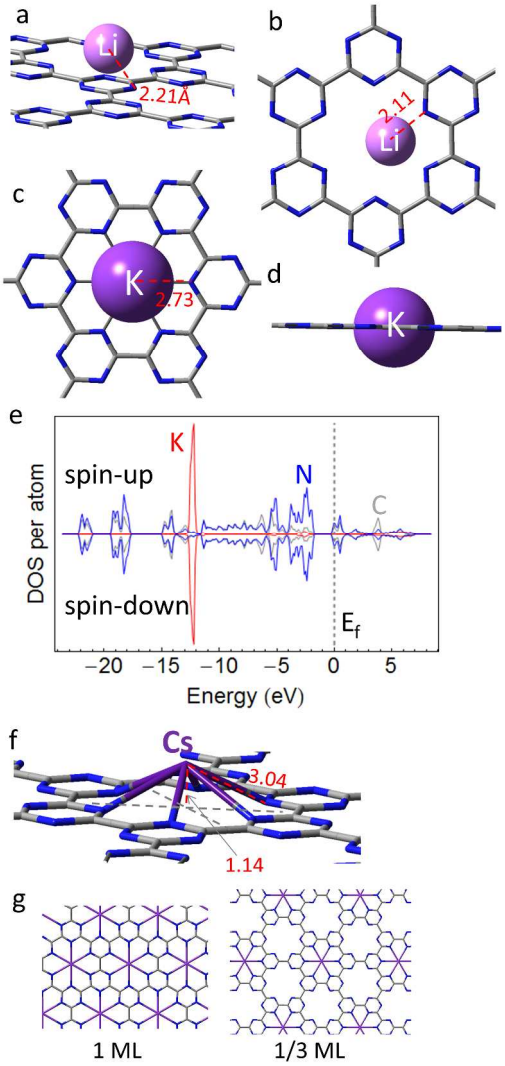

Figure 4.Metal atoms binding to the CN layer. (a) Li binding over s-triazine ring. (b) Li binding over the hexagonal pore. (c) Top view of K binding in the pore. (d) Side view of K binding in the pore. (e) Spin polarized local density of states plot of K-CN complex (PW91 results) at 1 ML of K coverage. (f) Cs binding over the pore. (g) Representative adsorbate coverages studied. K-CN as an example. All the red numbers are in Å. Metal atoms are presented in ball and stick model using van der Waals radii except for Cs.

In order to provide a rough estimation of relative binding strength, we calculated the binding energies of metal atoms to the layer. All the references use metal's bulk energy value (Table 2, binding energy column). The binding energy loosely indicates the σ-accepting and the π-backbonding capability of the metal atoms: the strongest binding energy can be achieved by metals which are considered as good π-donors. As shown in Table 2, the bindings for alkali and alkaline earth metals are energetically favourable, echoing the fact that these metals are highly reactive and easy to lose their *s* electrons. It can be observed clearly in Figure 4e, K 3*s* orbitals is deeply buried in metal's valence orbitals. The binding with metal changes the CN layer into metals, as it can be seen in the local density of states plot of the K-CN complex (Figure 4e). The Fermi energy is in the antibonding p_z-π* bands of C and N atoms. This is also true for Sc and Zr, which neighbour group II elements. On the other side, for noble metals, the binding energy compared is endothermic from 1.1 to 2.6 eV, reflecting their less reactive nature. Particularly, for the remaining elements (Fe, Ni, and, Cu), the low endothermic binding energy implies that the metal-CN structure could be prepared through processes like metal vapour deposition.

We have also carefully examined effects of supercell size on the binding energy. Due to the large size of the hexagonal pore (7.1 Å), effects of lateral interactions between adsorbed metal atoms in terms of binding energy are usually less than 0.1 eV. For example, at 1/3 ML and 1 ML coverages of CN (Figure 4g), the binding energy of K over the CN network is -3.21 and -3.20 eV, respectively.

The uniform pore distribution, the large pore-pore distance, and the rigid planar geometry indicate that the CN network is a good support for single-atom catalysis.[50] Furthermore, the magnetic moments are large for Ru and Fe, however, the pore size determines that the magnetic coupling is much weaker than their bulk form, which may be useful for making novel magnetic materials.[51, 52]

Conclusions

In summary, we have designed a simple 2D structure composed of C and N at 1:1 ratio, which can be viewed as formed by trimerization and polymerization of s-triazine units.

(1) The structure is flat and rigid in the *z* (out-of-plane) direction due to the proper distances between in-plane nitrogen lone-pairs. The single-layer CN is a typical wide bandgap semiconductor, which has uniformly distributed hexagonal pores in the layer with the van der Waals diameter of about 2.4 Å.

(2) This 2D single-layer structure is a good candidate for sieving hydrogen gas from other bigger molecular gases which is relevant to important chemical processes like syngas/natural gas production. The selectivity of H_2 gas against both CO_2 (10^{23}:1) and CH_4(10^{12}:1) is very high and the H_2 penetration frequency is estimated up to 10^8/s.

(3) Metal atoms of various sizes bind strongly to the pore position, converting the semiconducting material into metal. Since the electronic structure of the layer is greatly changed, the metal's catalytic activity must be influenced, thus it would be very interesting to continue the study on some real catalytic reactions.

Moreover, the 2D structure can be cut into 1D chain or quantum dots, though proper edge passivation is needed. Folding

the 2D layer into a nanotube or using the s-triazine-based hexagon as units to build Bucky ball are also plausible. These novel structures are to be explored.

Acknowledgments

Financial support was by 973 Programs of China (2014CB644003 and 2012CB619402) and by National Science Foundation of China (21203143 by c.w. and 21202129 by p.l.). We acknowledge computational resources at Materials Physics Center and Center of Microstructure Science of FIST, Xi'an Jiaotong University.

Notes and references

[a]*Frontier Institute of Science and Technology and State Key Laboratory for Mechanical Behavior of Materials, Xi'an Jiaotong University, Xi'an, Shaanxi 710054, China. Fax: 8629-8339 5364; Tel: 8629-8339 5364; E-mail: lipengfei@mail.xjtu.edu.cn; chaowu@mail.xjtu.edu.cn*

1. K. S. Novoselov, A. K. Geim, S. V. Morozov, D. Jiang, Y. Zhang, S. V. Dubonos, I. V. Grigorieva and A. A. Firsov, *Science*, 2004, **306**, 666-669.
2. L. S. Panchakarla, K. S. Subrahmanyam, S. K. Saha, A. Govindaraj, H. R. Krishnamurthy, U. V. Waghmare and C. N. R. Rao, *Adv. Mater.*, 2009, **21**, 4726-4730.
3. D. Usachov, O. Vilkov, A. Grüneis, D. Haberer, A. Fedorov, V. K. Adamchuk, A. B. Preobrajenski, P. Dudin, A. Barinov, M. Oehzelt, C. Laubschat and D. V. Vyalikh, *Nano Lett.*, 2011, **11**, 5401-5407.
4. H. J. Xiang, B. Huang, Z. Y. Li, S. H. Wei, J. L. Yang and X. G. Gong, *Phys. Rev. X*, 2012, **2**, 011003.
5. X. Luo, J. Yang, H. Liu, X. Wu, Y. Wang, Y. Ma, S.-H. Wei, X. Gong and H. Xiang, *J. Am. Chem. Soc.*, 2011, **133**, 16285-16290.
6. L. Song, Z. Liu, A. L. M. Reddy, N. T. Narayanan, J. Taha-Tijerina, J. Peng, G. Gao, J. Lou, R. Vajtai and P. M. Ajayan, *Adv. Mater.*, 2012, **24**, 4878-4895.
7. A. Y. Liu and M. L. Cohen, *Science*, 1989, **245**, 841-842.
8. C. Niu, Y. Z. Lu and C. M. Lieber, *Science*, 1993, **261**, 334-337.
9. A. Y. Liu and R. M. Wentzcovitch, *Phys. Rev. B*, 1994, **50**, 10362-10365.
10. E. G. Gillan, *Chem. Mater.*, 2000, **12**, 3906-3912.
11. J. Gracia and P. Kroll, *J. Mater. Chem.*, 2009, **19**, 3013.
12. M. J. Bojdys, J. Jeromenok, A. Thomas and M. Antonietti, *Adv. Mater.*, 2010, **22**, 2202-2205.
13. A. Y. Liu and M. L. Cohen, *Phys. Rev. B*, 1990, **41**, 10727-10734.
14. Z. J. Zhang, S. Fan, J. Huang and C. Lieber, *J. Electron. Mater.*, 1996, **25**, 57-61.
15. T. Y. Ma, S. Dai, M. Jaroniec and S. Z. Qiao, *Angew. Chem. Int. Ed.*, 2014, **53**, 7281-7285.
16. P. Kuhn, M. Antonietti and A. Thomas, *Angew. Chem. Int. Ed.*, 2008, **47**, 3450-3453.
17. J. Roeser, K. Kailasam and A. Thomas, *ChemSusChem*, 2012, **5**, 1793-1799.
18. P. Katekomol, J. Roeser, M. Bojdys, J. Weber and A. Thomas, *Chem. Mater.*, 2013, **25**, 1542-1548.
19. A. I. Cooper, *Adv. Mater.*, 2009, **21**, 1291-1295.
20. S. Ren, M. J. Bojdys, R. Dawson, A. Laybourn, Y. Z. Khimyak, D. J. Adams and A. I. Cooper, *Adv. Mater.*, 2012, **24**, 2357-2361.
21. S. Hug, M. B. Mesch, H. Oh, N. Popp, M. Hirscher, J. Senker and B. V. Lotsch, *J. Mater. Chem. A*, 2014, **2**, 5928.
22. W. Zhang, C. Li, Y.-P. Yuan, L.-G. Qiu, A.-J. Xie, Y.-H. Shen and J.-F. Zhu, *J. Mater. Chem.*, 2010, **20**, 6413.
23. L.-M. Tao, F. Niu, D. Zhang, T.-M. Wang and Q.-H. Wang, *New J. Chem.*, 2014, **38**, 2774.
24. S. Hug, M. E. Tauchert, S. Li, U. E. Pachmayr and B. V. Lotsch, *J. Mater. Chem.*, 2012, **22**, 13956.
25. M. J. Bojdys, J.-O. Müller, M. Antonietti and A. Thomas, *Chem. Eur. J.*, 2008, **14**, 8177-8182.
26. G. Kresse and J. Furthmüller, *Phys. Rev. B*, 1996, **54**, 11169-11186.
27. G. Kresse and J. Furthmüller, *Comput. Mater. Sci.*, 1996, **6**, 15-50.
28. J. P. Perdew, J. A. Chevary, S. H. Vosko, K. A. Jackson, M. R. Pederson, D. J. Singh and C. Fiolhais, *Phys. Rev. B*, 1992, **46**, 6671-6687.
29. J. P. Perdew and Y. Wang, *Phys. Rev. B*, 1992, **45**, 13244-13249.
30. P. E. Blöchl, *Phys. Rev. B*, 1994, **50**, 17953-17979.
31. G. Kresse and D. Joubert, *Phys. Rev. B*, 1999, **59**, 1758-1775.
32. J. Heyd, G. E. Scuseria and M. Ernzerhof, *J. Chem. Phys.*, 2003, **118**, 8207-8215.
33. J. P. Perdew, K. Burke and M. Ernzerhof, *Phys. Rev. Lett.*, 1996, **77**, 3865-3868.
34. S. Grimme, *J. Comput. Chem.*, 2006, **27**, 1787-1799.
35. While the 1×1 supercell represents only one occupancy (100% or 1 monolayer, ML). The $\sqrt{3} \times \sqrt{3}$ supercell provides 1/3, 2/3, and 1 ML adsorbate coverages. All pores (composed of six triazine units as a big hexagon) are occupied by adsorbates is 100% or 1 ML coverage.
36. http://periodictable.com/index.html, Accessed 10.29.2014. Lattice constants of Li, K, Rb, Cs, Ba, Sc, Zr, Fe, Ru, Ir, Ni, Pd, Pt, Cu, and Au are set to: 3.510, 5.328, 5.585, 6.141, 5.028, 3.309 (c 5.273), 3.232 (c 5.147), 2.867, 2.706 (c 4.282), 3.839, 3.524, 3.891, 3.924, 3.615, and 4.078 Å, respectively.
37. G. Henkelman, B. P. Uberuaga and H. Jónsson, *J. Chem. Phys.*, 2000, **113**, 9901-9904.
38. P. Zhu and V. Meunier, *J. Chem. Phys.*, 2012, **137**, 244703.
39. E. S. Penev, S. Bhowmick, A. Sadrzadeh and B. I. Yakobson, *Nano Lett.*, 2012, **12**, 2441-2445.
40. H. Tang and S. Ismail-Beigi, *Phys. Rev. Lett.*, 2007, **99**.
41. D.-e. Jiang, V. R. Cooper and S. Dai, *Nano Lett.*, 2009, **9**, 4019-4024.
42. B. M. Wong and S. H. Ye, *Phys. Rev. B*, 2011, **84**, 075115.
43. D. Josa, J. Rodríguez-Otero, E. M. Cabaleiro-Lago and M. Rellán-Piñeiro, *Chem. Phys. Lett.*, 2013, **557**, 170-175.
44. Y. Jiao, A. Du, M. Hankel, Z. Zhu, V. Rudolph and S. C. Smith, *Chem. Commun.*, 2011, **47**, 11843.
45. H. Liu, V. R. Cooper, S. Dai and D.-e. Jiang, *J. Phys. Chem. Lett.*, 2012, **3**, 3343-3347.
46. P. Matter, L. Zhang and U. Ozkan, *J. Catal.*, 2006, **239**, 83-96.
47. Y. Zhao, R. Nakamura, K. Kamiya, S. Nakanishi and K. Hashimoto, *Nat. Commun.*, 2013, **4**.
48. F. Gao, G.-L. Zhao, S. Yang and J. J. Spivey, *J. Am. Chem. Soc.*, 2013, **135**, 3315-3318.
49. J. C. Slater, *J. Chem. Phys.*, 1964, **41**, 3199-3204.
50. X.-F. Yang, A. Wang, B. Qiao, J. Li, J. Liu and T. Zhang, *Acc. Chem. Res.*, 2013, **46**, 1740-1748.

51. Y.-Z. Zheng, G.-J. Zhou, Z. Zheng and R. E. P. Winpenny, *Chem. Soc. Rev.*, 2014, **43**, 1462-1475.
52. Y.-Z. Zheng, Z. Zheng and X.-M. Chen, *Coord. Chem. Rev.*, 2014, **258–259**, 1-15.

TOC

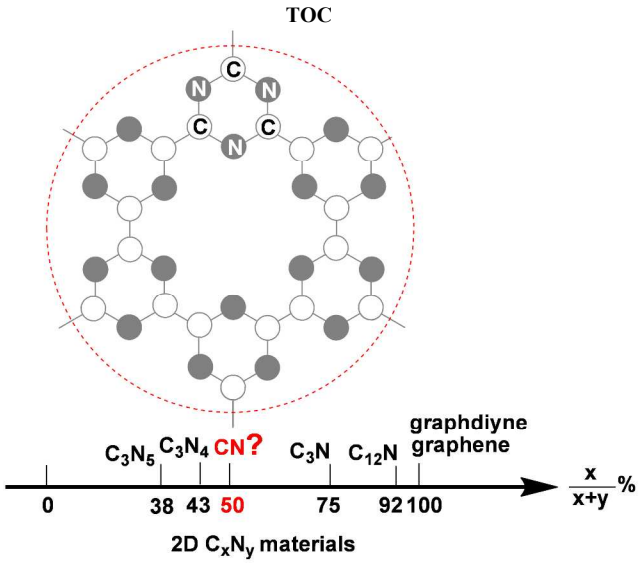

Using the first-principles simulations, we predicate a 2D CN(1:1) network and explore its potential applications in electronics, gas separation, and catalysis.